



Journal of Catalysis Vol. 263, No. 1, 2009

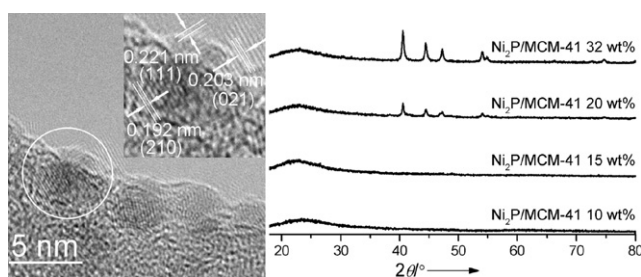
Contents

PRIORITY COMMUNICATION

Alternative synthesis of bulk and supported nickel phosphide from the thermal decomposition of hypophosphites

pp 1–3

Qingxin Guan, Wei Li*, Minghui Zhang, Keyi Tao



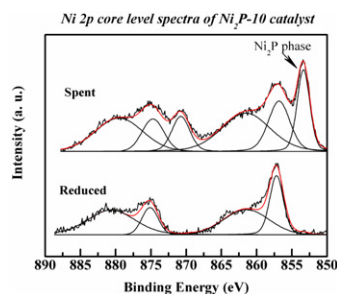
The synthesis of nickel phosphide has been achieved by a heat treatment of nickel chloride and sodium hypophosphite at 300 °C followed by reduction at 500 °C.

REGULAR ARTICLES

A novel method for preparing an active nickel phosphide catalyst for HDS of dibenzothiophene

pp 4–15

J.A. Cecilia, A. Infantes-Molina, E. Rodríguez-Castellón, A. Jiménez-López*

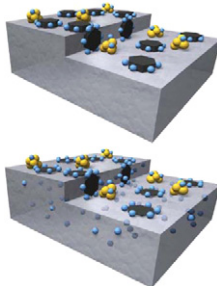


$\text{Ni}_2\text{P}/\text{MCM-41}$ catalysts were prepared by H_2 -TPR through a novel method using nickel(II) dihydrogenphosphite, $\text{Ni}(\text{HPO}_3\text{H})_2$, as a precursor salt. The formation of more Ni_2P phase takes place with time on stream.

Structural characterization of Ni–W hydrocracking catalysts using in situ EXAFS and HRTEM

pp 16–33

S.D. Kelly, N. Yang, G.E. Mickelson, N. Greenlay, E. Karapetrova, W. Sinkler, Simon R. Bare*

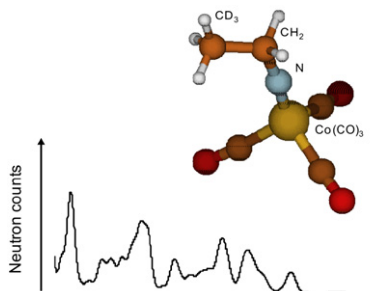


Schematic models of the two sulfided Ni–W catalysts.

Identification of reaction intermediates during hydrogenation of CD₃CN on Raney-Co

pp 34–41

Peter Schäringer, Thomas E. Müller*, Andreas Jentys, Johannes A. Lercher

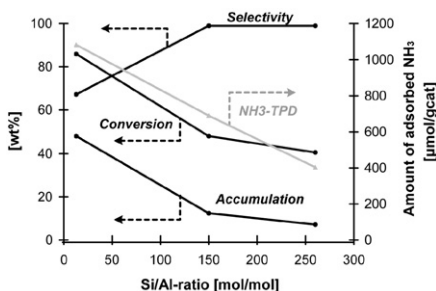


By inelastic neutron scattering (INS), a nitrene was identified as likely reaction intermediate formed on the surface of Raney-Co after co-adsorption of acetonitrile and hydrogen.

Beckmann-rearrangement of cyclododecanone oxime to ω -laurolactam in the gas phase

pp 42–55

W. Eickelberg, W.F. Hoelderich*

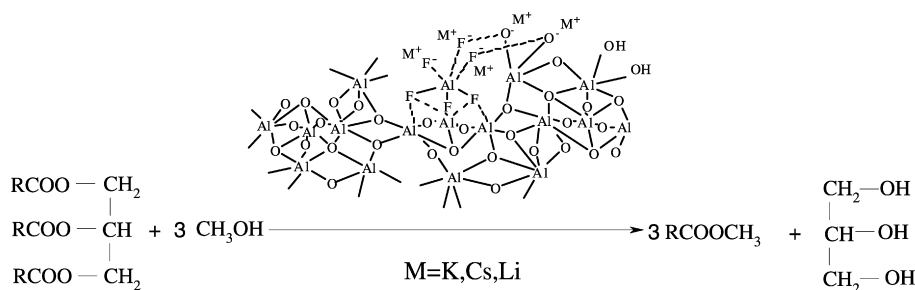


This paper investigates the heterogeneously catalysed Beckmann-rearrangement of cyclododecanone oxime to ω -laurolactam in the gas phase. Using an acid treated [Al,B]-BEA zeolite at a temperature of approx. 320 °C and reduced pressures, complete conversion and a selectivity of 98% were achieved.

Transesterification of vegetable oils on basic large mesoporous alumina supported alkaline fluorides—Evidences of the nature of the active site and catalytic performances

pp 56–66

Marian Verziu, Mihaela Florea, Simion Simon, Viorica Simon, Petru Filip, Vasile I. Parvulescu*, Christopher Hardacre*

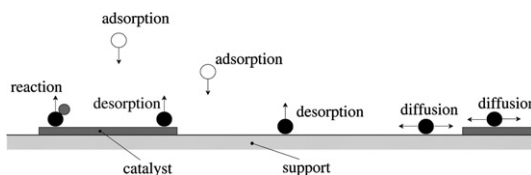


Transesterification of vegetable oils on KF, LiF and CsF/Al₂O₃ catalysts under thermal, microwave and ultrasounds activation.

Effects of diffusion and particle size in a kinetic model of catalyzed reactions

pp 67–74

T.G. Mattos, Fábio D.A. Aarão Reis*

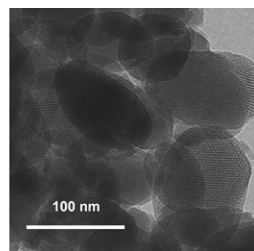
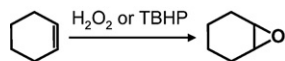


In a simple model of reaction, diffusion, adsorption and desorption, the conditions for a net flux of reactants from the support to the catalyst are determined, with significant increase of the turnover frequency for small particles.

Direct room-temperature synthesis of methyl-functionalized Ti-MCM-41 nanoparticles and their catalytic performance in epoxidation

pp 75–82

Kaifeng Lin, Paolo P. Pescarmona*, Kristof Houthoofd, Duoduo Liang, Gustaaf Van Tendeloo, Pierre A. Jacobs

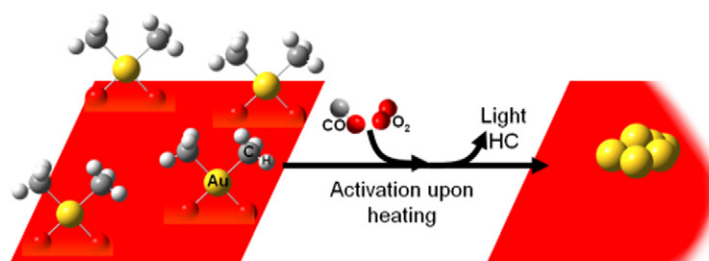


Methyl-functionalized Ti-MCM-41 nanoparticles display improved catalytic performance in the epoxidation of cyclohexene.

Activation of dimethyl gold complexes on MgO for CO oxidation: Removal of methyl ligands and formation of catalytically active gold clusters

pp 83–91

Yalin Hao, Bruce C. Gates*



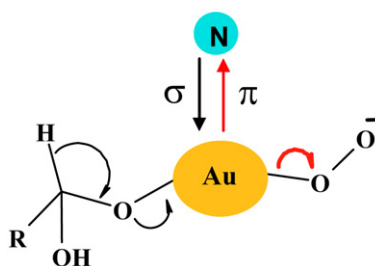
EXAFS: Cluster formation, XANES: Gold positively charged

EXAFS: Cluster formation. XANES: Gold positively charged.

Selective deactivation of gold catalyst

pp 92–97

Cristina Della Pina, Ermelinda Falletta, Michele Rossi*, Adriano Sacco

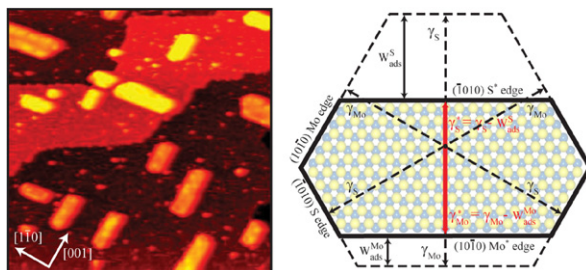


The progressive poisoning effect of different molecules on carbon supported gold catalysts has been evaluated during the aerobic oxidation of glucose. The kinetics of catalyst deactivation has been interpreted by considering the important contribute of electronic factors which overlap the space shielding of active sites, due to long range poison-catalyst interaction influencing the entire metal particle.

Scanning tunneling microscopy studies of TiO₂-supported hydrotreating catalysts: Anisotropic particle shapes by edge-specific MoS₂-support bonding

pp 98–103

Jakob Kibsgaard, Bjerne S. Clausen, Henrik Topsøe, Erik Lægsgaard, Jeppe V. Lauritsen*, Flemming Besenbacher

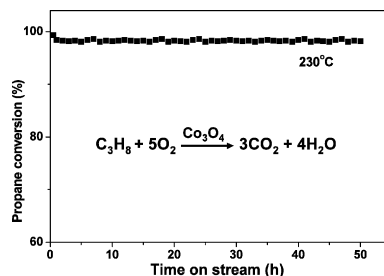


Using high-resolution scanning tunneling microscopy, the role of distinct particle-support interactions present only at the particle edges is investigated for titania-supported MoS₂ nanoparticles, which are used as hydrotreating catalyst.

Dry citrate-precursor synthesized nanocrystalline cobalt oxide as highly active catalyst for total oxidation of propane

pp 104–113

Qian Liu, Lu-Cun Wang, Miao Chen, Yong Cao*, He-Yong He, Kang-Nian Fan

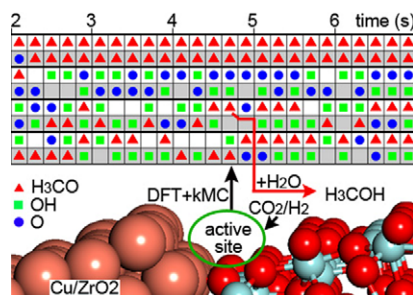


Nanocrystalline Co_3O_4 prepared by soft reactive grinding exhibited excellent activity and high stability for propane combustion. Complete conversion has been achieved at reaction temperatures as low as 230 °C.

CO_2 fixation into methanol at Cu/ZrO₂ interface from first principles kinetic Monte Carlo

pp 114–122

Qian-Lin Tang, Qi-Jun Hong, Zhi-Pan Liu*

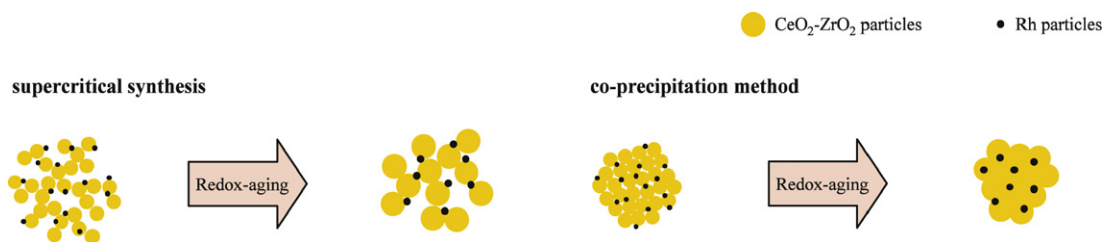


DFT based kinetic Monte Carlo simulation of CO_2 fixation to methanol over Cu/ZrO₂ reveals that hydrolysis is a key step in producing methanol and that the interfacial Cu is partially oxidized during reaction.

Characteristics of CeO₂–ZrO₂ mixed oxide prepared by continuous hydrothermal synthesis in supercritical water as support of Rh catalyst for catalytic reduction of NO by CO

pp 123–133

Jeong-Rang Kim, Wan-Jae Myeong, Son-Ki Ihm*

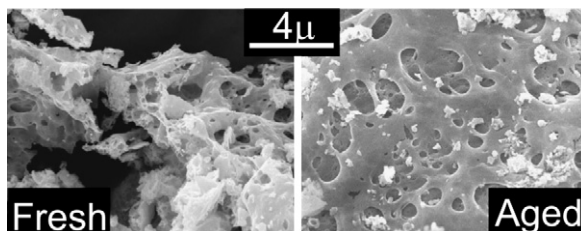


Ceria–zirconia mixed oxide supports prepared in supercritical water show superior thermal stability.

Surface chemistry and reactivity of ceria–zirconia-supported palladium oxide catalysts for natural gas combustion

pp 134–145

Stefania Specchia*, Elisabetta Finocchio, Guido Busca, Pietro Palmisano, Vito Specchia



The deactivation 2% Pd/CeO₂–ZrO₂ catalyst upon severe sulfur-hydrothermal ageing is due to the progressive oxidation of highly dispersed Pd nanoparticles to PdO_x, as well as their coalescence.

Catalysts based on platinum–tin and platinum–gallium in close contact for the selective hydrogenation of cinnamaldehyde

pp 146–154

A.J. Plomp, D.M.P. van Asten, A.M.J. van der Eerden, P. Mäki-Arvela, D.Yu. Murzin, K.P. de Jong, J.H. Bitter*

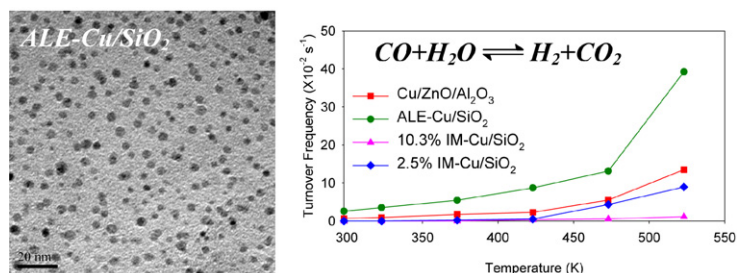


Platinum–tin catalysts were prepared via (A) impregnation and (B) reductive deposition precipitation. Via (A), a Pt–Sn interaction was absent while via (B) close interaction was observed, thereby enhancing catalytic selectivity.

Active sites on Cu/SiO₂ prepared using the atomic layer epitaxy technique for a low-temperature water–gas shift reaction

pp 155–166

Ching-Shiun Chen *, Jarrn-Horng Lin, Tzu-Wen Lai, Bao-Hui Li

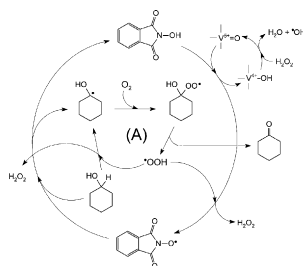


An ALE-Cu/SiO₂ catalyst (Cu/SiO₂ prepared by an atomic layer epitaxy method) has higher activity than an impregnated Cu catalysts (IM-Cu/SiO₂) in the water–gas shift reaction.

Mechanistic investigation of the catalytic system based on *N*-hydroxy-phthalimide with vanadium co-catalysts for aerobic oxidation of alcohols with dioxygen

pp 167–172

Paweł Jarosław Figiel, Jarosław Marek Sobczak*

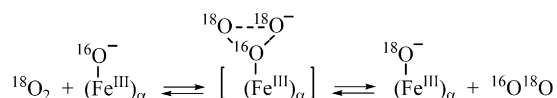


A mechanism for the aerobic oxidation of alcohols with dioxygen catalyzed by NHPI and vanadium complexes is proposed. Its essential step is generation of a phthalimide-*N*-oxyl (PINO*) radicals as result of reaction of NHPI with oxovanadium(V) compounds. The oxidation of alcohols concerns both radical and molecular pathways.

O₂ isotopic exchange in the presence of O[−] anion radicals on the FeZSM-5 surface

pp 173–180

M.V. Parfenov, E.V. Starokon, S.V. Semikolenov, G.I. Panov*

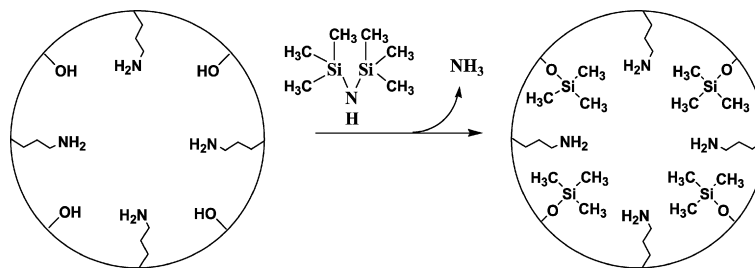
Mechanism R₀: E = 0.8 kJ/mol (198–298 K)Mechanism R₁: E = 15 kJ/mol (223–448 K)

High reactivity of O[−]/FeZSM-5 species (α -oxygen) in the oxidation of methane, benzene and other substrates at room temperature is well known. This work reveals high reactivity of α -oxygen in isotopic exchange with O₂ at 198–448 K.

Acid–base cooperativity in condensation reactions with functionalized mesoporous silica catalysts

pp 181–188

Sarah L. Hruby, Brent H. Shanks*

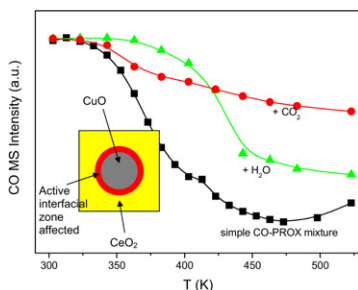


Acid–base cooperativity in the Knoevenagel condensation reaction was found for amine-functionalized mesoporous silica catalysts operating through either an imine intermediate or ion-pair mechanism. The role of silanols as weak acids rather than through hydrogen bonding was demonstrated using different solvents.

Preferential oxidation of CO in rich H₂ over CuO/CeO₂: *Operando*-DRIFTS analysis of deactivating effect of CO₂ and H₂O

pp 189–195

Daniel Gamarra, Arturo Martínez-Arias *

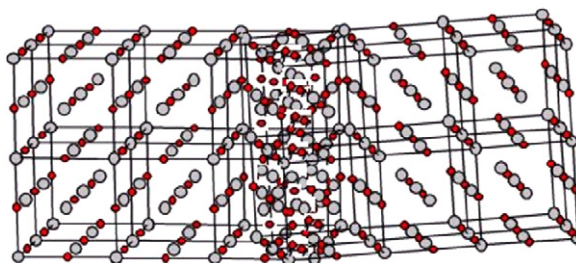


The deactivating effects of CO₂ and H₂O on CO-PROX performance of a CuO/CeO₂ catalyst are examined by *operando*-DRIFTS.

Grain boundary control in nanocrystalline MgO as a novel means for significantly enhancing surface basicity and catalytic activity

pp 196–204

Roxana Vidruk, Miron V. Landau *, Moti Herskowitz, Michael Talianker, Nahum Frage, Vladimir Ezersky, Natali Froumin



Atomic disorder formed at grain boundaries between jointed nanocrystals in MgO material as a result of precursor densification is a source of coordinative unsaturated ions associated with surface basic sites.

RESEARCH NOTE**Heterogeneously catalyzed selective *N*-alkylation of aromatic and heteroaromatic amines with alcohols by a supported ruthenium hydroxide**

pp 205–208

Jung Won Kim, Kazuya Yamaguchi, Noritaka Mizuno*



The *N*-alkylation of various aromatic and heteroaromatic amines with alcohols could efficiently be promoted by an easily prepared supported ruthenium hydroxide catalyst Ru(OH)_x/Al₂O₃.